

MCPNS: A Macropixel Collocated Position and Its Neighbors Search for Plenoptic 2.0 Video Coding

Vinh Van Duong, Thuc Nguyen Huu, Jonghoon Yim, and Byeungwoo Jeon

Abstract—Compared with a traditional unfocused plenoptic 1.0 camera, a newly introduced focused plenoptic 2.0 camera with effective light field sampling can capture images at much higher spatial resolutions. However, due to difference in the optical structures of the two cameras, the existing fast motion estimation (ME) method for plenoptic 1.0 videos is expected to be sub-optimal for encoding plenoptic 2.0 videos. Here, we describe the primary differences in motion characteristic between plenoptic 1.0 and 2.0 videos and propose a new fast ME method, macropixel collocated position and its neighbors search (MCPNS) for plenoptic 2.0 videos. We propose reducing the number of macropixel collocated position (MCP) search candidates based on new observations of center-biased motion-vector distribution at macropixel resolutions. Due to large motion deviation behavior around each MCP location in plenoptic 2.0 videos, we propose selecting key MCP locations with the lowest matching cost to perform a neighbors MCP search that improves motion search accuracy. Compared with existing methods, ours achieves superior performance without prior knowledge of the orientation of the microlens array. Simulations confirm the effectiveness of the proposed algorithm in both bitrate savings and computational costs. The code for our method can be found at <https://github.com/duongvinh/MCPNS>.

Index Terms— Light field, plenoptic camera, video coding, fast motion estimation, macropixel image.

I. INTRODUCTION

Light field (LF) imaging captures both the directions and intensities of light rays, from the scene to an observer, using a plenoptic camera. As shown in Fig. 1(a), a conventional camera

Vinh Van Duong, Thuc Nguyen Huu, Jonghoon Yim, and Byeungwoo Jeon (corresponding author) are with the Digital Media Laboratory (DMLAB), Department of Electrical and Computer Engineering, Sungkyunkwan University, 2066 Seoburo, Jangan-gu, Suwon, 16410, KOREA (email: bjjeon@skku.edu).

This work was supported in part by Basic Science Research Program (RS-2023-00208453) through the National Research Foundation of Korea (NRF) and by the ICT Creative Consilience Program (IITP-2023-2020-0-01821) supervised by the IITP (Institute for Information & communications Technology Planning & Evaluation), both funded by the Ministry of Science and ICT, Korea.

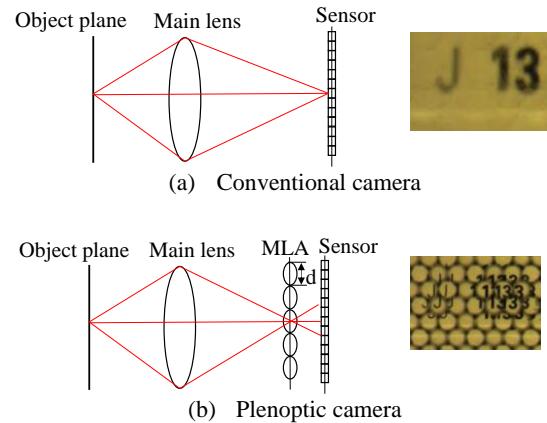


Fig. 1. Illustrations of the conceptual optical structures for conventional and plenoptic cameras. (a) A conventional camera captures only the average intensity of light rays hitting an image sensor. (b) With an MLA element, a plenoptic camera can capture both the intensity of light rays and their direction to produce a macropixel image pattern.

only captures the average intensity of light rays hitting camera sensors, and the directions of light rays are lost. In contrast, a plenoptic camera, in which a microlens array (MLA) is placed in front of the image sensor plane, can record not only the intensity but also the direction of the light rays, as shown in Fig. 1(b). The image response in the camera sensor created with an MLA is referred to as a macropixel or lenslet image. With this unique optical structure, images or videos captured by a plenoptic camera provide much richer and more valuable information for applications such as depth estimation, point cloud data processing, and saliency detection [1].

Because the intensity distribution of a plenoptic image or video is markedly different from that of conventional images and videos, additional care should be paid to reducing spatial and temporal redundancies and maintaining fidelity in plenoptic imagery [2]–[28]. While a comprehensive survey of coding solutions for plenoptic images can be found in [29]–[30], plenoptic video coding has become a new research topic, receiving significant attention recently from those working with MPEG-Immersive encoding [31]–[43]. More importantly, because the sole commercially available plenoptic 1.0 camera (e.g., Lytro Illum camera) is currently not on the market, the

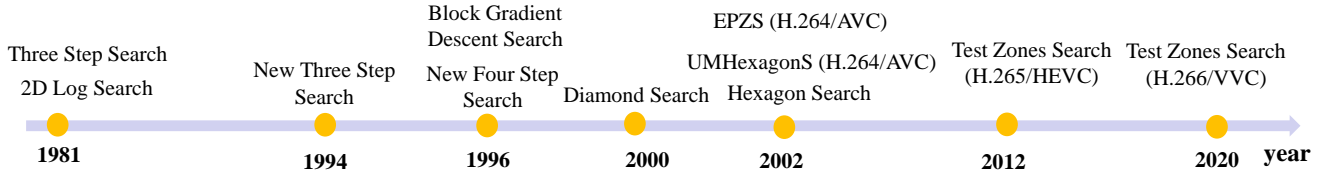


Fig. 2. Milestones of fast motion estimation methods for encoding conventional videos, for which the TZS method is currently adopted for the reference software of most recent standard video encoders, such as H.265/HEVC or H.266/VVC.

research community is focusing on plenoptic 2.0 cameras (e.g., Raytrix camera), which can provide more flexible control of the trade-off between spatial and angular resolutions. By considering the distinct intensity distribution of plenoptic 2.0 images, several new intra-coding tools [8]-[9], [26]-[27] that are designed for and target encoding plenoptic 2.0 images have been introduced. However, inter-coding tools (e.g., motion estimation (ME)) for plenoptic 2.0 video have yet to be investigated closely.

In dealing with video data, and inter-coding algorithms in particular, ME is an effective tool for finding the best, most similar block in already-encoded frames and therefore reducing temporal redundancy. Additionally, ME generates a motion vector (MV), which is the displacement between the best-matched block and the current prediction. Although a full search (FS) provides the best quality among various ME algorithms, its computational complexity is high. As shown in Fig. 2, numerous simpler search patterns [44]-[52] have been introduced to overcome the limitations of the FS method. Recently, the test zones search (TZS) [53] method has been adopted for standard encoders (e.g., H.265/HEVC and H.266/VVC) and now represents the state-of-the-art for fast ME in conventional video. In short, the assumptions related to designing a fast ME method employing TZS for conventional video need to be re-scrutinized for plenoptic video because the complex intensity distribution and MVs of plenoptic cameras differ from those of conventional counterparts.

Table I presents works related to fast ME for plenoptic video coding. For plenoptic 1.0 videos, Li *et al.* [54] first proposed macropixel-based fast ME (denoted MFME), suggesting that the searching candidates should follow a macropixel collocated position (MCP) search pattern due to its optimal motion concentration. Later, they provided technical proposals [41]-[43] for MPEG-Immersive coding, which also integrates many tools for lenslet video into HEVC or VVC reference software. Another academic paper, described in our previous work [56], proposed microlens-based test zones search (MTZS) for plenoptic 1.0 videos, which adds a searching step to conventional TZS to standardize microlens image distances. A technical proposal for MTZS in MPEG-Immersive coding can be found in [57]. Regarding fast ME for plenoptic 2.0 videos, a more suitable fast search method should be considered an optical structure for plenoptic 2.0 because of its differences from plenoptic 1.0. Taking this into account, Yang *et al.* [58] proposed a micro-image-based two-step search (MTSS) method for plenoptic 2.0 videos recently. It includes microlens-diameter and matching-distance spatial search as the first step search to exploit correlations among microlens images due to the distinct optical structure of plenoptic 2.0 imagery.

TABLE I
WORKS RELATED TO THE FAST MOTION ESTIMATION FOR
PLENOPTIC VIDEO ENCODING

Categories	Related Works	
	Technical Proposal for MPEG-immersive	Academic papers
Plenoptic 1.0 Videos	[41]-[43], [57]	[54]-[55], [56]
Plenoptic 2.0 Videos	[59]-[68]	[58]

Additionally, region-limited TZS can be employed as a local refinement search in the second step.

In this paper, we argue that, despite its ability to capture better motion accuracy compared to those existing works in MFME [41] and MTZS [56], the MTSS [58] may still fail to achieve optimal results when encoding plenoptic 2.0 videos. Due to the focused MLA structure, the micro-image patterns captured by plenoptic 2.0 cameras tend to repeat in both current and several neighboring microlenses by following the matching pixel distance (denoted as s). Therefore, the MTSS [58] leverages this matching pixel distance to define additional search candidates helping to capture more accurate matching block in ME search processes. However, it should be noted that the MTSS [58] employed a single matching pixel parameter “ s ” that represents for whole video sequence, which may not be able to handle video sequences with complex scenes or motion (e.g., video sequences with different depth of field or fast motion generated by movement of the camera or object). Although several updates and improvements with more accurate matching pixel parameters are reported in a technical proposal for MPEG-Immersive encoding [59]-[63], the pre-defined search candidates based on matching pixel distance (s) in MTSS [58] might still limit the efficiency of this method.

In short, since the plenoptic 2.0 camera has unique optical structures compared to plenoptic 1.0 camera, it generates more complex motion behavior resulting in the existing methods still showing their limitations in estimating an accurate optimal MV. We therefore propose a new macropixel collocated position and its neighbors search for plenoptic 2.0 video coding (denoted MCPNS). By conducting statistical analysis of the motion distribution, we still observe that the optimal MVs are mainly located at around MCP locations same as in the case of plenoptic 1.0 videos, but we further point out there is a large portion of optimal MV deviation occurs around each MCP location in plenoptic 2.0 videos. Taking this into account, we propose a joint search approach by adding extra neighbor search candidates around each MCP location to handle the large MV deviation problem. This is the main distinction from existing

methods (MFME [54] and MTSS [58]) that allow us to capture more accurate optimal MVs at the macropixel-level searching stage in plenoptic 2.0 videos. It appears to be a relatively simple yet effective method based on our rigorous analysis and understanding of the motion characteristics of plenoptic 2.0 videos. Moreover, the idea of a joint search approach (MCP and its neighbors search) at the macropixel-level searching stage is conceptually novel as there are no existing academic papers on fast ME for plenoptic 2.0 videos that provide clear theoretical and statistical analyses of the motion difference between plenoptic 1.0 and 2.0 videos.

Preliminary results of this paper are reported in MPEG-Immersive standardization [66]-[68]. Specifically, the concept of a neighbors MCP search was introduced in [66] to help improve motion accuracy, and a fast MCP search pattern based on center-biased assumption at the macropixel level was introduced in [67] to reduce encoding time. In this paper, we provide comprehensive analyses of our proposed method as well as introduce several improvements to control the trade-off between coding performance and encoding time complexity. In short, the contributions of our paper are summarized as follows:

- Unlike existing methods, we theoretically discuss the main assumptions on the effects of scene motion captured by plenoptic cameras. To validate these assumptions, we provide a statistical analysis of MV distributions for both conventional and plenoptic videos and describe the main differences between them.
- We present a new fast ME called MCPNS, which contains a joint search approach between MCP and its neighbors MCP search locations to handle large motion deviation at the macropixel level search stage in plenoptic 2.0 videos.
- To reduce the time complexity of ME in the case of a large window search, we introduce a fast MCP search pattern based on a motion center-biased assumption and fast neighbors MCP search only for the top K -MCP position containing the lowest distortion cost.
- Our method is more generalized than others as it performs an MLA orientation-agnostic MCP search pattern to address different MLA orientations of plenoptic 2.0 cameras.

The remainder of this paper is organized as follows. Section II describes the four-dimensional (4D) LF motion properties and the motion-distribution characteristics of each model of plenoptic camera. Section III presents our proposed fast search MCPNS for plenoptic 2.0 video coding in detail. Section IV evaluates the performance, and our conclusions are provided in Section V.

II. 4D LIGHT FIELD MOTION PROPERTIES AND ITS STATISTICAL ANALYSIS

This section presents background information on the optical structures of plenoptic cameras and the LF motion characteristics recorded in a 4D LF sensor camera. We also statistically analyze the MV distributions of conventional and plenoptic videos and point out the main differences between them.

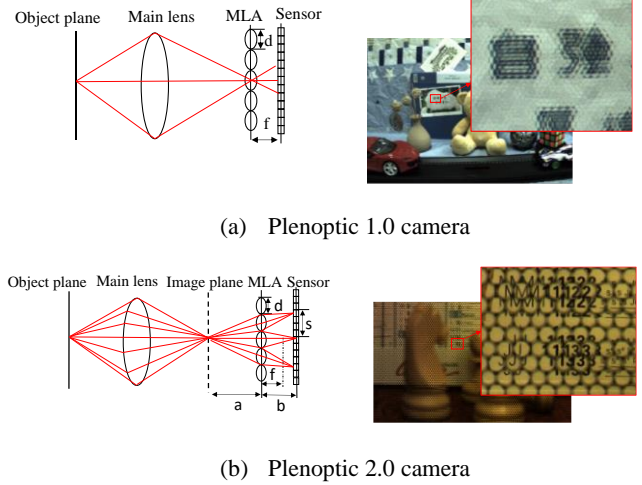


Fig. 3. The optical structures and real macropixel images captured by plenoptic 1.0 and plenoptic 2.0 cameras [9], [70].

A. Structure and Characteristics of Plenoptic Cameras

As shown in Fig. 3(a), a plenoptic 1.0 camera has an MLA at the image plane of the main camera lens, with the photosensor camera one focal length behind the microlens. The main lens is focused on a distance of one focal length in front of the microlens and the MLA is focused at infinity. As a result, all pixels under the microlens correspond to a single spatial object point, which comes from a direction specific to that pixel, as shown on the right side of Fig. 3(a). Images from a plenoptic 1.0 camera are rendered by integrating all angular samples at a particular spatial point. However, because each spatial point is sampled by a single microlens, rendering involves integrating all the pixels in each micro-image. As designed, we only can take one pixel per microlens in a plenoptic 1.0 camera, resulting in a rendered image with very low resolution.

Unlike a plenoptic 1.0 camera, a plenoptic 2.0 camera is based on a microlens array focused on the image plane of the main lens, as shown in Fig. 3(b). Each microlens captures a portion of the image formed by the main lens. The sensor can be considered as being moved back, away from the main lens, so that the image forms some distance in front of the microlenses. The MLA serves as an array of real cameras, reimaging parts of the image onto the sensor. Each microlens forms a relay imaging system with the main camera lens. The position of each microlens satisfies the lens equation, $1/a + 1/b = 1/f_m$, where a is the distance between the MLA and the image plane of the main lens, b is the distance between the MLA and camera sensor, and f_m is the focal length of the microlens. Using the geometric distance, the distance between the pixel's response on the sensor from the same object point, s , can be calculated using Equation (1) for plenoptic 2.0 cameras operating in the Keplerian mode (the Raytrix R5 and Raytrix R8 models) or Equation (2) for plenoptic 2.0 cameras operating in the Galilean mode (a Tsinghua single focused camera) [8], [70]:

$$s = \frac{a - b}{a} \times d \quad (1)$$

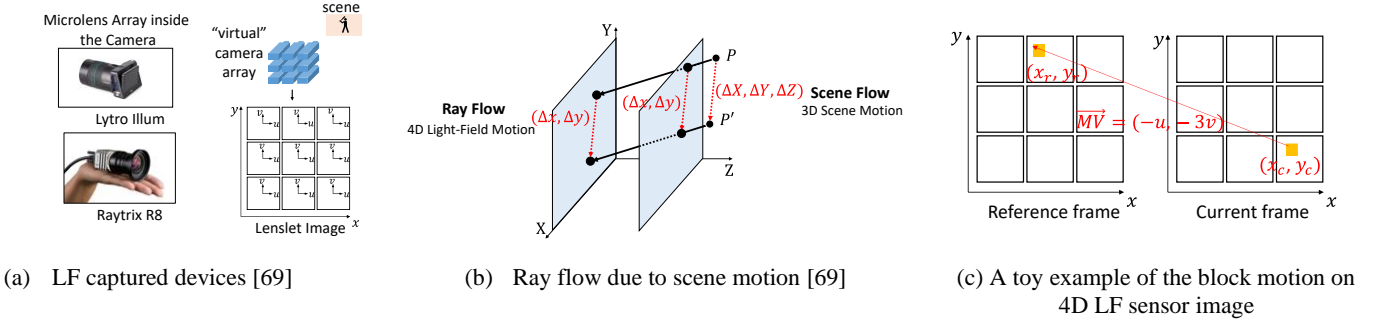


Fig. 4. Ray flow due to scene motion in a light field camera sensor image. (a) Plenoptic cameras with the microlens array work as a virtual camera array. (b) Motion of the scene point that emits or reflects the ray results in a change in the (x, y) coordinates of the ray, but the (u, v) coordinates remain constant. (c) A toy example showing the block motion (translation) in the current frame at (x_c, y_c) to the reference frame at (x_r, y_r) with step sizes of u and v in vertical and horizontal coordinates.

$$s = \frac{a+b}{a} \times d \quad (2)$$

where d is the diameter of each microlens, depending on the plenoptic camera model. Comparing the optical design of the plenoptic 2.0 camera with that of a plenoptic 1.0 camera lead to several key conclusions:

- Due to the relay image system in a plenoptic 2.0 camera, the spatial angular resolution is not fixed by the number of microlenses. This means that the angular samples for a given spatial point are sampled by different microlenses, which enables higher spatial resolution compared with a plenoptic 1.0 camera. In other words, rendering with plenoptic 2.0 camera data involves integrating across microlens images rather than within images, as is done in a plenoptic 1.0 camera. As a result, a plenoptic 2.0 camera can capture LF images at a much higher spatial resolution compared with a plenoptic 1.0 camera.
- Because there is a major difference between the optical structures of plenoptic 1.0 and 2.0 cameras, paying attention to pixel intensity distributions can help design a more effective search algorithm suitable for each type of camera. In short, plenoptic 2.0 video coding is a new topic that has received significant attention from MPEG-Immersion coding teams [31]-[34], [39]-[43]. However, further investigation is required to design an effective coding method that efficiently compresses these kinds of data according to different acquisition devices.

B. Effect of Scene Motion on Ray Motion Recorded on Plenoptic Camera Sensors

In this section, we briefly revisit the ray flow equation proposed in [69], which describes the relationship between the *scene flow* (three-dimensional [3D] scene motion) and the *ray flow* (ray motion recorded in a sensor camera). We can interpret *ray flow* as the change $(\Delta x, \Delta y)$ in a light ray coordinate due to the change in scene motion as $\Delta \mathbf{X} = (\Delta X, \Delta Y, \Delta Z)$ using 3D spatial coordinates. Moreover, because our goal is to estimate a two-dimensional (2D) MV in block-based video coding, which is simpler than estimating the dense 3D scene flow in [69], we rely primarily on these important properties of the ray flow equation to gain insight into our video coding problem.

Given the 3D scene point P at location \mathbf{X} and the time instance t , then $\mathbf{X}' = \mathbf{X} + \Delta \mathbf{X}$ is the location of point P at time instance $t + 1$, where $\Delta \mathbf{X} = (\Delta X, \Delta Y, \Delta Z)$ is the difference

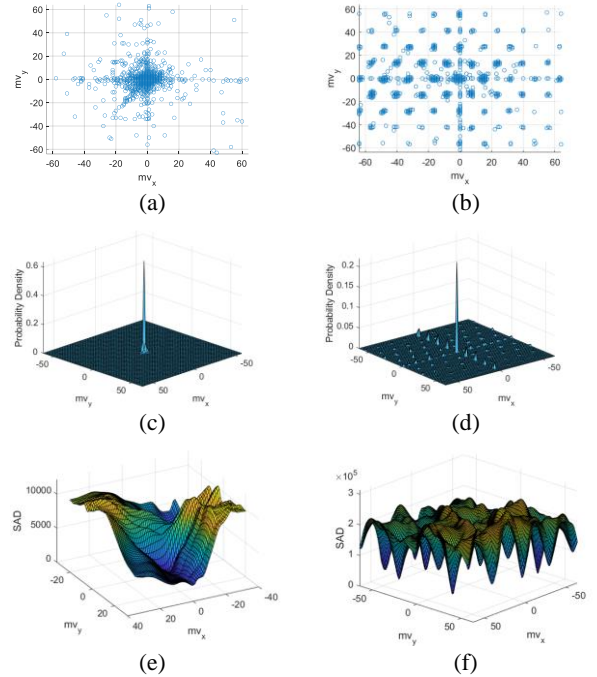


Fig. 5. Illustration of typical MV distributions and matching error surfaces between conventional (left side) and plenoptic (right side) videos: the MV distribution map (first row), the probability density distribution of MV (second row), and the matching error surface distribution (third row).

between the 3D scene point locations. The main assumption is that if we only consider the translation motion of the scene patch, the rays move parallel to themselves (i.e., the $[u, v]$ coordinates of the ray remain constant). As shown in Fig. 4(a), a 4D LF sensor image can be presented as a 2D array of pinhole cameras (i.e., a 2D array of microlens). In this representation, (u, v) is the pixel index within individual microlens and (x, y) is the location of the cameras. To be self-contained, we recap the main assumptions of the 3D scene motion recorded in sensor images of plenoptic cameras found in [69], as follows:

- As shown in Fig. 4(b), a light ray shifts horizontally or vertically across microlens images, where the amount of shift $(\Delta x, \Delta y)$ is independent of the ray's original coordinates. In other words, rays maintain the same pixel index (u, v) after motion but in different microlens images

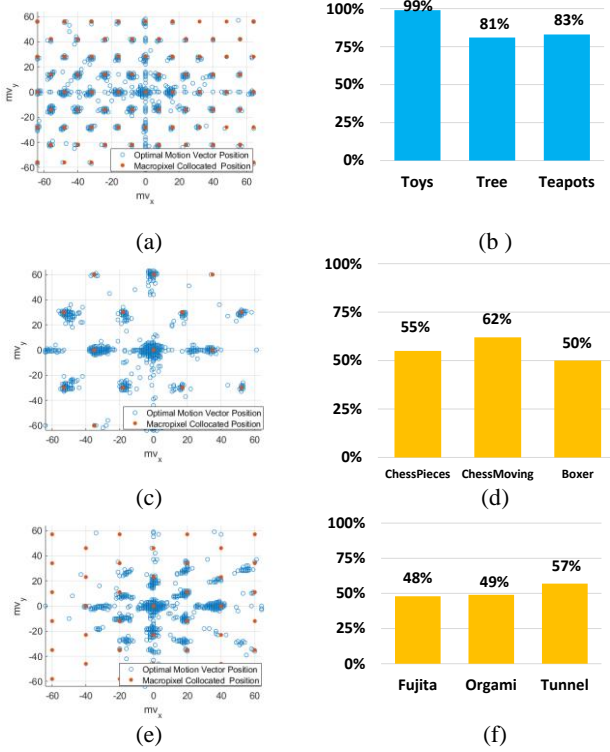


Fig. 6. Statistical analyses of MV distributions of a plenoptic 1.0 camera (Lytro Illum; in the first row) and plenoptic 2.0 cameras (Raytrix R8 and Raytrix R5; in the second and third rows, respectively). The MVs are plotted together with MCP locations (denoted as red points) in the first column, and the proportion of the optimal MV located at the same location as MCP is shown in the second column.

(x, y) ; this is the case because the scene motion results in rays being translated parallel to themselves. This is the *most important characteristic* that we need to pay attention to, as highlighted by the key difference between scene motions recorded with the 2D conventional sensor image versus our 4D LF sensor image.

- As shown in Fig. 4(c), which depicts a toy example of translation motion on the 4D LF sensor camera, block motion only changes the (x, y) coordinates; the (u, v) coordinates remain unchanged, moving with a **step size of u and v** in horizontal and vertical coordinates. Based on this observation, we can analyze the MV distribution for a video captured by a plenoptic camera and use the resulting insights to design an effective search pattern for each type of plenoptic camera.

C. Statistical Analysis and Motivation

To analyze the differences in motion characteristics between conventional and plenoptic videos, VVC reference software VTM-11.0 [74] was used for encoding. In the case of conventional video, several standard video sequences were tested, and their detailed properties are described in the common test condition document [73]. For plenoptic video test sequences, we used video sequences captured by three different kinds of plenoptic cameras, (Lytro Illum, Raytrix R5, and Raytrix R8). We encoded the first 30 frames of each test sequence using the default configuration in the low-delay main

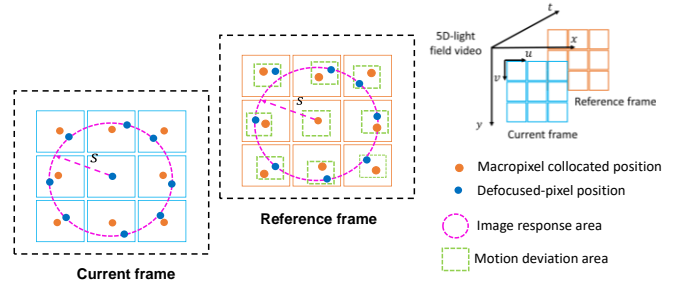


Fig. 7. A toy example illustrates different types of pixel similarity that can be found by the motion estimation process, where we can see that the inter-pixel similarity varies in a larger angular window search range for the case of plenoptic 2.0 videos.

(LD-main) profile. A full search was used to obtain the optimal MV with a search range of 64. Our main observations are presented in detail below.

Unique motion distribution of plenoptic videos compared with conventional videos: In Fig. 5(a)–(d), the MV distribution of conventional video is primarily located in the center search area, where the distribution of motion, in the case of a plenoptic camera, is notably sparse and dispersed across the search window. This is a consequence of the MLA elements, where the motion caused by camera/object movement is sampled by the MLA at a resolution equal to the nearest distance between these microlenses. In Fig. 5(e)–(f), the sum absolute difference in the block-matching process is calculated, providing the difference in the intensity distribution between conventional and plenoptic video sequences. Notably, the unimodal error surface assumption no longer holds true for the plenoptic video. In essence, the TZS method, originally designed based on these assumptions, yields significantly inferior results when applied to encoding plenoptic videos. This motivated us to design a new fast search pattern tailored specifically for plenoptic videos.

Optimal motion vectors are located primarily at MCPs: In the first column of Fig. 6, the optimal MVs are plotted together with the MCP locations for different camera models, where each red dot corresponds to the location of one microlens in the MLA placed in front of the camera sensor. It should be noted that the MLA layout arrangement is different for each plenoptic camera model. For example, Lytro Illum and Raytrix R8 cameras exhibit a horizontal MLA layout arrangement, whereas the Raytrix R5 employs a vertical MLA layout arrangement. The optimal MVs are located primarily around the MCP points and distributed sparsely all over the search window; this is different from conventional MVs, which are only located around the predicted motion vector (pMV), which surrounds the center of the window search area. Additionally, we attempted to calculate the percentage of optimal MVs located exactly at MCP locations (second column of Fig. 6). Specifically, we found that the optimal MVs were often located exactly at MCP locations more than 80% of the time for a plenoptic 1.0 camera (Lytro Illum), while plenoptic 2.0 cameras (Raytrix R8 and R5 camera models) exhibited a lower incidence of similarly positioned MVs, ranging from 50% to 60%. Due to the strong concentration of optimal MVs at these MCPs, we can utilize these MCPs as the initial search candidates in the fast ME algorithm for plenoptic videos.

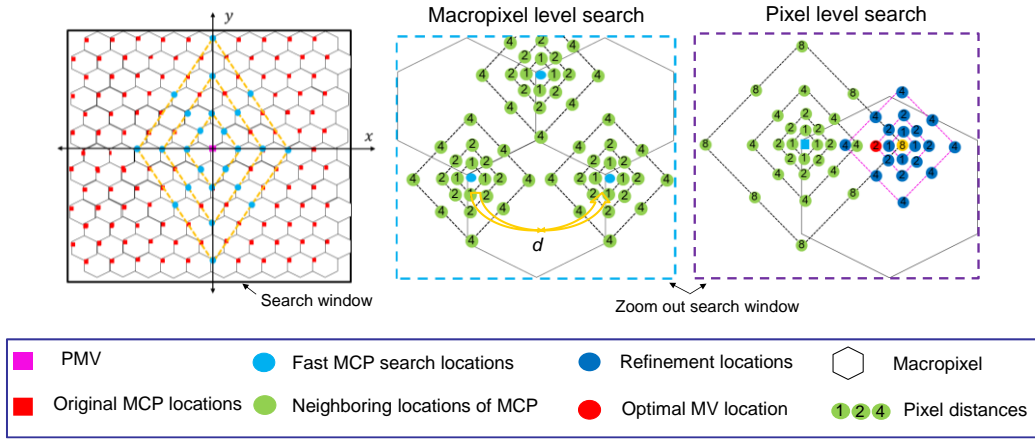


Fig. 8. Overview of our proposed fast ME for plenoptic 2.0 videos which incorporates search patterns tailored to address the motion characteristics of at both macropixel and pixel search levels. Here, we are assuming the video sequences are captured by a plenoptic camera with a horizontal MLA orientation.

A large portion of motion deviation occurred around each MCP search location in plenoptic 2.0 videos: Because the optical configuration differs between plenoptic 1.0 and plenoptic 2.0 cameras, a significant deviation was observed between the optimal MVs and their MCPs in plenoptic 2.0 cameras; the deviation was smaller for the plenoptic 1.0 camera. This highlights the reason why the MFME[54]/MTSS[58] do not prove effective when applying a fast search for encoding our plenoptic 2.0 videos. In other words, if we only perform the search process on these MCP positions, as is done in MFME[54]/MTSS[58], this cannot guarantee that we will find an optimal MV since fewer optimal MVs are located at exactly these MCP locations in plenoptic 2.0 cameras compared with plenoptic 1.0 cameras. The large motion deviation around each MCP location is the most crucial and distinctive motion characteristic of plenoptic 2.0 videos when compared to their plenoptic 1.0 counterparts.

In Fig. 7, we present an additional illustrative example to delve deeper into the similarity of pixels in the motion search process of plenoptic 2.0 video coding. Because each microlens is treated as a virtual camera that records the same scene from a different perspective, the pixel similarity of a micro-image may be easily found in a neighboring microlens by following the macropixel distance values, as denoted in orange in Fig. 7. However, because a plenoptic 2.0 camera is unfocused, each microlens records part of an object and creates the defocused microlens imaging pattern in the camera sensor. The defocused micro-image is spread over several neighboring microlenses following the matching pixel distance (s), as shown in Equations (1) and (2). More importantly, the value of parameter s is not constant but varies depending on the specific characteristics of each video sequence, such as disparity range or depth of field. In summary, similar to plenoptic 1.0 videos, the inter-pixel similarity in plenoptic 2.0 videos is primarily influenced by camera/object movements with a step size of macropixel resolution in the horizontal and vertical coordinates. However, inter-pixel similarity in a plenoptic 2.0 video is additionally affected by larger defocused-pixel similarity variation. This motivated us to design a new search pattern to handle the larger motion deviation around each MCP location in the case of ME of plenoptic 2.0 videos.

III. PROPOSED METHOD

In this section, we introduce the proposed search patterns for each search stage in detail, and describe how our method can estimate more accurate block MVs compared with state-of-the-art methods.

A. Search Locations Addressing Highly Optimal Motion Vectors Located at Macropixel Collocated Positions (MCPs)

Original MCP search pattern: As pointed out in Section II.B, the motion distribution of plenoptic videos is located primarily at MCP locations, where the light rays shift across microlenses, generating the motion displacement at the macropixel resolution. To reflect this unique characteristic, we found that the initial motion search pattern should align with these MCP locations. The main difference in the motion characteristics of plenoptic videos, as compared to conventional videos, is that block motion in plenoptic videos is shifted by one or multiple macropixel resolution, while in conventional videos, block motion is only shifted by pixel resolution. This implies that a search pattern based on the TZS method, designed for conventional motion searches at the pixel-level resolution, would be inadequate to accommodate the larger motion steps at the macropixel-level resolution seen in plenoptic videos.

As depicted in Fig. 8, we can derive the MCP locations from the center of search window by following the macropixel diameter (d). For simplicity, we describe how to define the position of MCP candidates in the horizontal MLA orientation in a process similar to the case of vertical MLA orientation. In detail, we can denote $h = \sqrt{3} d/2$ and $w = d$ as the distance between two adjacent microlenses in the horizontal and vertical directions. Given the window search range (W), we can determine the location of MCP search candidates using Equation (3), as shown below [54],[58]:

$$\begin{aligned} x &= \begin{cases} p \cdot w + \frac{w}{2}, & q \in O \\ p \cdot w, & q \in E \end{cases} \\ y &= q \cdot h \end{aligned} \quad (3)$$

with $p \in \Phi, q \in \Psi$, and $(x, y) \in [-W, W]$

where (x, y) represents the coordinates of each MCP candidate within the search range. O and E represent sets of odd and even numbers, respectively. Additionally, (Φ, Ψ) denotes the set number of macropixel inside the searching range area (W) in the horizontal and vertical coordinates. The total number of MCP candidates inside the given search range can be computed as follows [54],[58]:

$$\psi_1 = \begin{cases} (m+1) \cdot \left(2 \left\lfloor \frac{W}{w} \right\rfloor + 1\right) + 2m \left\lfloor \frac{W+w/2}{w} \right\rfloor, & m \in E \\ m \cdot \left(2 \left\lfloor \frac{W}{w} \right\rfloor + 1\right) + 2(m+1) \left\lfloor \frac{W+w/2}{w} \right\rfloor, & m \in O \end{cases} \quad (4)$$

$$m = \left\lfloor \frac{W}{h} \right\rfloor$$

Fast MCP search pattern addressing the center-biased assumption at the macropixel level: As illustrated in Fig. 9, rather than examining all MCP locations as defined in Equation (3), we introduce a fast MCP search pattern that allows us to speed up encoding time, especially when dealing with large search window. To be more precise, we observed that the optimal MV density distribution in the plenoptic video adheres to a center-biased assumption at the macropixel-level resolution. This is a fundamental distinction from the MV distribution in traditional videos, which typically follows a center-biased assumption at the pixel-level resolution. In our approach, the calculation of the number of fast MCP search candidates ($\hat{\psi}_1$) is as follows:

$$\hat{\psi}_1 = \sum_{i=1}^M 8, i \leq M \text{ with } M = \left\lfloor \frac{W}{d} \right\rfloor, \quad (5)$$

where W and d are the search window size and microlens diameter, respectively. Furthermore, given the relatively large macropixel size, our search step is increased to the maximum value of M , following a linear-scale order, as opposed to the log2-scale order utilized in the TZS method. Thanks to our fast MCP search approach, the number of fast MCP candidates is considerably smaller than its original MCP candidates (i.e., $\hat{\psi}_1 \ll \psi_1$). For example, ψ_1 consists of 1307 MCP locations calculated using Eq. (4) for the Raytrix R5 camera, with $d = 23$ and $W = 384$. By employing our fast MCP search approach, the actual fast MCP candidates are significantly reduced (e.g., $\hat{\psi}_1 = \left\lfloor \frac{384}{23} \right\rfloor \times 8 = 128$).

MLA orientation-agnostic MCP search pattern addressing different MLA orientations: Figures 10(c)-(d) show two kinds of MCP patterns depending on MLA orientation. The MLA arrangement is not necessarily the same overall LF cameras. For example, the MCP locations of the Raytrix R8 camera follow the horizontal MLA orientation in Fig. 10(a), while those of the Raytrix R5 and Single Focused cameras use a vertical MLA orientation in Fig. 10(b). Taking this into account, our method in previous technical contributions in MPEG-Immersive [66], [67] requires knowledge of MLA orientations in advance to properly predefine the MCP search locations, whereas the MTSS [58] needs to rotate the given image clockwise by 90° through preprocessing if the MLA orientation is not horizontally arranged, as it is in a Raytrix R5 and the single focused camera. In short, our previous works [66], [67] and MTSS [58] need prior

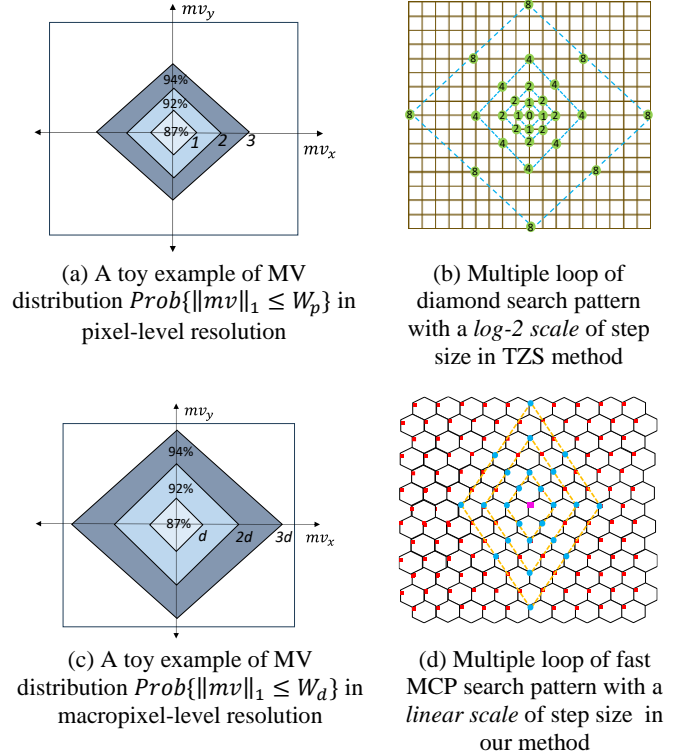


Fig. 9. Illustration of the MV density distribution following the center-biased assumption at pixel-level resolution and macropixel-level resolution at the top and bottom, respectively.

knowledge of MLA orientation or preprocessing of rotation before performing the actual ME procedures.

Furthermore, camera users typically have full freedom to take photos in either portrait or landscape mode. It may not be practically feasible to assume that the MLA orientation of a given LF image is known in advance. Moreover, when a video is edited by mixing several sources or cuts to form a picture, the MLA orientations inside one picture cannot be even assumed to be the same. In this respect, the conventional fast ME method (e.g., TZS [53]) is also agnostic to camera or content orientation; that is, it does not require prior information on whether the video was captured in portrait or landscape mode. It is therefore advisable to design a fast motion search algorithm for LF video that is agnostic to MLA orientation. Figures 10(c)-(d) illustrate two fast MCP search patterns, characterized by hexagonal or rhomboid shapes. As this search needs to be performed in both horizontal and vertical MLA orientations, the number of fast MCP candidates only increased by double compared to a single fast MCP search approach in Eq. (5).

B. Search Locations Addressing Large Portions of Optimal Motion Vector Deviation Around Each MCP

Neighbors MCP search pattern: Drawing upon the insights presented in Section II.B, we incorporate a neighbors MCP search into our method. This addition enables us to effectively address large motion deviations occurring around these MCP locations in plenoptic 2.0 videos. The number of neighbor candidates at each MCP location can be calculated as follows:

$$\psi_2 = 4 + \sum_{i=2}^N 8, i \leq N \text{ with } N = \log_2(d), \quad (6)$$

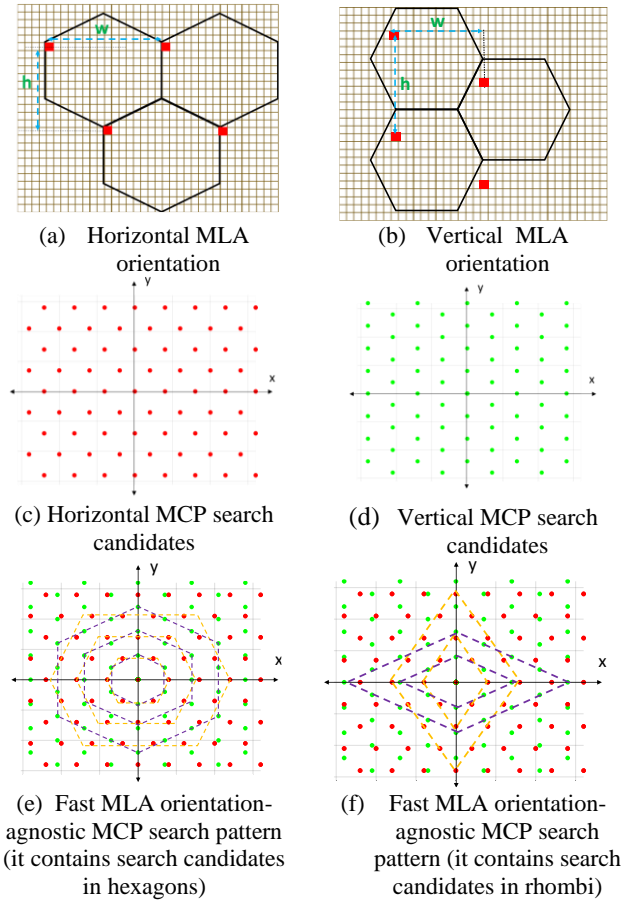


Fig. 10. Illustrations of our proposed fast MLA orientation-agnostic MCP search pattern which can accommodate either MLA layout of horizontal or vertical MLA orientations in various plenoptic 2.0 camera model.

where i depends on the searching distance in N loops of the diamond search pattern, as shown in Fig. 8. The search window of the neighbors MCP search is equivalent to the microlens diameter (d). This algorithm uses a small diamond shape consisting of four checking points for the first loop and a large diamond shape with eight checking points for the remaining loops. As indicated in Table II, a significant proportion of optimal motion vectors (MVs) can be located in the surrounding area of each MCP location within an 8-pixel search window. If we could not find a new best MV within the 8-pixel distance (i.e., after every three search loops), we apply an early termination strategy to eliminate redundant searches.

Fast neighbors MCP search approach: A straightforward approach is to perform the neighbors MCP search at all MCP locations, which can demand significant computational resources. Instead of performing the neighbor search at all fast MCP locations ($\hat{\psi}_1$), we selected the top K number of MCP candidates among $\hat{\psi}_1$ MCP locations with the lowest BMD values to perform the neighbors MCP search. For example, in this paper, we empirically chose $K = 16$, which is much smaller than the original fast MCP locations (e.g., $\hat{\psi}_1 = 256$ in the last step). The neighbors MCP search is executed sequentially at each MCP position until the last K MCP location

TABLE II
PERCENTAGE (%) OF OPTIMAL MOTION VECTORS DEVIATED
AROUND EACH MCP LOCATIONS

SEQUENCES	BOXER	CHESSES	FUJITA	TUNNEL
$P \leq 1$	41%	45%	53%	60%
$P \leq 2$	62%	65%	75%	85%
$P \leq 4$	88%	84%	90%	95%
$P \leq 8$	96%	93%	95%	98%

is reached. The total number of search points for this neighbors MCP search step amounts to $K \times \psi_2$.

Once the best MV at the macropixel motion resolution level has been determined, a finer motion search is conducted over a smaller grid around the current best MV candidate, as depicted in Fig. 8. In our approach, we employ the star-based refinement search pattern originally introduced in TZS [53] for conventional video coding to refine our pixel motion resolution search, where the search candidates required in this step is computed as follows:

$$\psi_3 = 4 + \sum_{i=2}^N 8, i \leq N \text{ with } N = \log_2(d), \quad (7)$$

where i depends on the searching distance in N loops of the diamond search. Finally, since we added extra $\hat{\psi}_1$ MCP candidates from another MLA orientation, compared to Eq. (5), the total number of search candidates required in our method in the best-case scenario can be computed as follows:

$$\Omega = 2\hat{\psi}_1 + K\psi_2 + \psi_3 \quad (8)$$

To make our method easier to understand, Fig. 11 presents the entire procedure of our proposed algorithm. More discussion of the distinction with the existing method can be found in the Supplemental file.

IV. EXPERIMENTAL RESULTS AND ANALYSIS

In this section, we describe the test conditions in detail, followed by the coding performance in terms of compression efficiency, computation complexity, and ablation study.

A. Test Conditions

As shown in Fig. 12, we used eleven plenoptic 2.0 videos from the MPEG-I public dataset [75], which were captured by three kinds of plenoptic 2.0 camera models: Raytrix R5, Raytrix R8, and Single Focused cameras. The proposed algorithm and other anchor methods were implemented on top of VVC reference software VTM 11.0 [74], using the quantization parameters in common test conditions [75]. We performed these experiments on servers running on the Windows 10 operating system, using an ADM Ryzen 9 3900X 12-Core Processor and 32 GB of DDR4 memory. We encoded and evaluated the performance under default settings in low-delay main (LD-main) and random access-main (RA-main) configurations. The rate-distortion performance was evaluated in terms of the Bjøntegaard delta bitrate (BDBR) [76], where a negative value denotes better compression performance compared with the anchor method. The peak signal-to-noise ratio in the BDBR was measured in the Y color channel. The

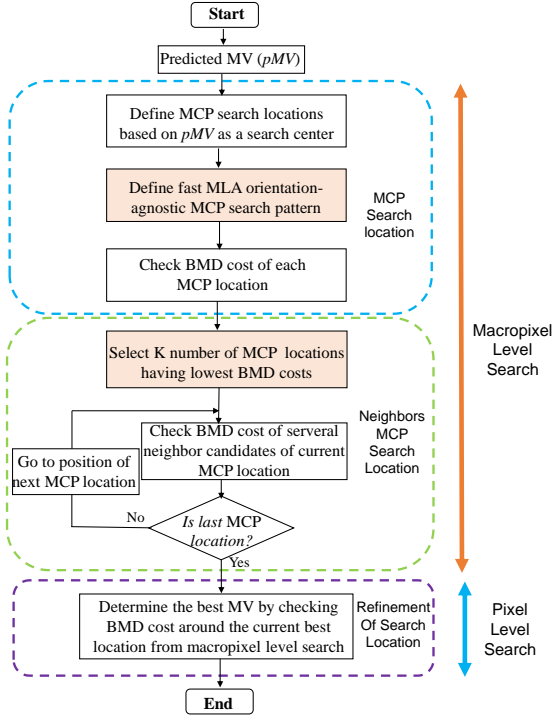


Fig. 11. An illustration of our proposed method, in which the fast search decision in each searching location is highlighted in orange.

encoding time ratio (ETR) computed for each video sequence was as follows:

$$ETR = \frac{\text{geomean}(T_m)}{\text{geomean}(T_{\text{anchor}})} \times 100 (\%) \quad (9)$$

where T_m and T_{anchor} are the geometric mean of the encoding time in four quantization values of method m and the anchor method, respectively.

To assess the effectiveness of our proposed method, several testing cases were defined in Table III. In addition to the TZS and FS methods, we compared our method with several state-of-the-art fast MEs for plenoptic videos, including the MFME [54] for plenoptic 1.0 videos and MTSS [58] for plenoptic 2.0 videos. The MFME [54] was originally designed for encoding plenoptic 1.0 video sequences in HEVC reference software, but we re-implemented this method in the VVC platform and modified it by setting the diameter of the microlens parameter according to the type of plenoptic 2.0 video sequence. The MTSS results were generated using an executable file provided by its authors. For making a fair comparison, all methods (FS, MFME [54], MTSS [58], and our MCPNS) only replaced the TZS method in the uni-predictive search process. That is, the performance of FS was optimal. This helped us determine the maximum performance that each method can achieve compared with the FS method.

B. Overall Performance of Proposed Method

Tables IV and V compare the performance of our proposed method and other methods in LD-main and RA-main conditions. We empirically set the default number of neighbors of MCP candidates $K = 16$. We compare the results with

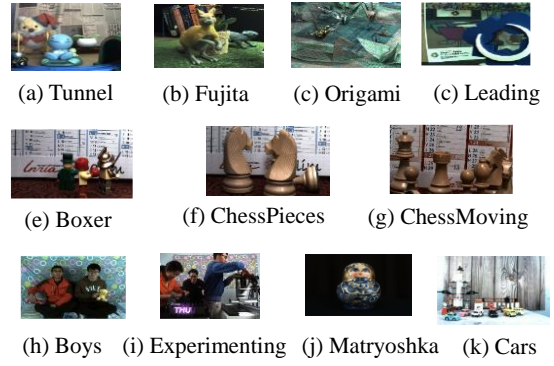


Fig. 12. Plenoptic 2.0 video sequences. (a)–(d): Raytrix R5 captured video sequences, (e)–(g): Raytrix R8 captured video sequences, and (h)–(k) Single Focused captured video sequences.

TABLE III
THE CODING SETTING OF TESTING CASES; OUR PROPOSED METHOD IS HIGHLIGHTED IN **BOLD**.

TESTING CASES	CODING TOOL CONFIGURATION SETTINGS
VVC	VTM 11.0 [58] with Main Profiles
FS	“VVC” + Full Search method [74]
TZS	“VVC” + TZS method [74]
MFME	“VVC” + MFME [54]
MTSS	“VVC” + MTSS [58]
MCPNS	“VVC” + Our proposed MCPNS

existing fast ME for plenoptic videos in two scenarios: with or without prior information on MLA orientation. From these results, we can observe several key conclusions as follows:

- Overall, our method surpasses the TZS method, yielding an average improvement of 3.37% and 2.54% in LD-main and RA-main conditions, respectively. The TZS algorithm exhibits decreased coding performance due to its suboptimal search location and strategy, originally designed for conventional videos. Notably, our method demonstrates superior coding performance compared to existing methods and closely matches the performance of the FS method.
- With the help of our MLA orientation-agnostic MCP search pattern, our method achieves significantly better coding performance compared to existing methods, particularly in scenarios where prior knowledge of MLA orientation is unavailable. For instance, our approach yielded coding gains of approximately 4.28% and 1.25% in LD-main, and 2.63% and 0.76% in RA-main conditions when compared to MFME/MTSS methods, respectively. This highlights the limitation of MFME/MTSS, which are primarily designed for encoding plenoptic video sequences with a horizontal MLA configuration and may struggle to address the vertical MLA configuration found in the Raytrix R5 and Single Focused camera models, as evidenced in Tables IV and V.
- When prior knowledge of MLA orientation is available, our method continues to deliver superior performance compared to MFME/MTSS. This advantage stems from our method's additional search process centered around MCP locations, which effectively handles the substantial

TABLE IV

THE PERFORMANCE COMPARISON OF FAST ME METHODS USING IN UNI-PREDICTIVE ME SEARCH WITH LD-MAIN CONDITIONS.

Camera model	Default MLA orientation	Sequences	Agnostic to MLA orientation	Without prior information of MLA orientation**		With prior information of MLA orientation		Agnostic to MLA orientation
			FS	MFME [54]	MTSS* [58]	MFME [54]	MTSS* [58]	MCPNS (Ours)
Raytrix R5	Vertical orientation	Tunnel	-3.82%	1.37%	-2.81%	-3.62%	-	-3.62%
		Fujita	-8.88%	4.85%	-3.85%	-7.15%	-	-8.34%
		Origami	-6.13%	2.71%	-0.96%	-5.05%	-	-5.23%
		Leading	-2.88%	5.49%	-1.59%	-2.65%	-	-2.68%
Raytrix R8	Horizontal orientation	Boxer	-3.35%	-2.90%	-2.58%	-2.90%	-2.58%	-3.19%
		ChessPieces	-8.01%	-7.53%	-7.60%	-7.53%	-7.60%	-7.50%
		ChessMoving	-5.08%	-3.41%	-3.67%	-3.41%	-3.67%	-4.03%
Single Focused	Vertical orientation	Boys	-0.85%	4.94%	0.21%	-0.53%	-	-0.65%
		Experiments	-1.01%	2.60%	-0.04%	-0.59%	-	-0.77%
		Cars	-0.24%	0.01%	0.00%	0.01%	-	-0.21%
		Matryoshka	-1.20%	1.88%	-0.38%	-0.86%	-	-0.80%
Avg. BD-rate			-3.77%	0.91%	-2.12%	-3.12%	-	-3.37%
Avg. Enc. Time Ratio			410%	99%	101%	99%	-	105%

*The results generated using an executable file provided by the authors

** It always assumes that the videos sequences captured by plenoptic camera with the horizontal MLA orientation

TABLE V

THE PERFORMANCE COMPARISON OF FAST ME METHODS USING IN UNI-PREDICTIVE ME SEARCH WITH RA-MAIN CONDITIONS.

Camera model	Default MLA orientation	Sequences	Agnostic to MLA orientation	Without prior information of MLA orientation**		With prior information of MLA orientation		Agnostic to MLA orientation
			FS	MFME [54]	MTSS* [58]	MFME [54]	MTSS* [58]	MCPNS (Ours)
Raytrix R5	Vertical orientation	Tunnel	-3.52%	0.37%	-2.93%	-3.43%	-	-3.38%
		Fujita	-4.02%	1.92%	-1.27%	-3.00%	-	-3.97%
		Origami	-5.40%	1.45%	-2.70%	-4.41%	-	-4.51%
		Leading	-3.71%	1.68%	-2.53%	-3.34%	-	-3.75%
Raytrix R8	Horizontal orientation	Boxer	-2.11%	-1.63%	-1.68%	-1.63%	-1.68%	-1.90%
		ChessPieces	-4.71%	-4.41%	-4.33%	-4.41%	-4.33%	-4.64%
		ChessMoving	-4.86%	-3.38%	-4.19%	-3.38%	-4.19%	-4.75%
Single Focused	Vertical orientation	Boys	-0.45%	2.57%	0.21%	-0.22%	-	-0.25%
		Experiments	-0.87%	1.40%	-0.04%	-0.50%	-	-0.64%
		Cars	-0.02%	-0.03%	0.01%	0.01%	-	-0.03%
		Matryoshka	-0.81%	1.04%	-0.11%	0.27%	-	-0.08%
Avg. BD-rate			-2.77%	0.09%	-1.78%	-2.19%	-	-2.54%
Avg. Enc. Time Ratio			1040%	100%	107%	99%	-	103%

*The results generated using an executable file provided by the authors

** It always assumes that the videos sequences captured by plenoptic camera with the horizontal MLA orientation

MV deviations in plenoptic 2.0 videos. Compared to MFME, our method yields coding improvements of approximately 0.25% and 0.35% in LD-main and RA-main conditions, respectively. Although the overall performance of MTSS in scenarios with prior MLA orientation information is not explicitly stated, we still observe that our method outperforms MTSS when encoding video sequences captured by the Raytrix R8 camera. In summary, given the lower coding efficiency of MFME/MTSS compared to FS, these methods may achieve suboptimal performance in the context of encoding plenoptic 2.0 videos when compared to our approach.

- In terms of time complexity, while our method did not attain the fastest encoding times compared to existing methods, it consistently demonstrated competitive performance. To be specific, our approach required approximately 3% more encoding time in LD-main and 5%

more in RA-main conditions when compared to the TZS method. This slight increase in encoding time can be attributed to our method's emphasis on the neighbors MCP search process, which aims to effectively handle significant motion deviations around MCP locations. With our innovative fast search approach in MCP and its neighboring MCP locations, our method successfully strikes a balance between coding performance and encoding time complexity.

C. Ablation Study

1) *Average of Number of Search Points (ASP) and Average Prediction Error (APE)*. To measure the complexity of ME, we calculated the average number of search points (ASP) for one ME as follows:

$$ASP = \frac{\sum_{i=1}^N SP(i)}{N} \quad (10)$$

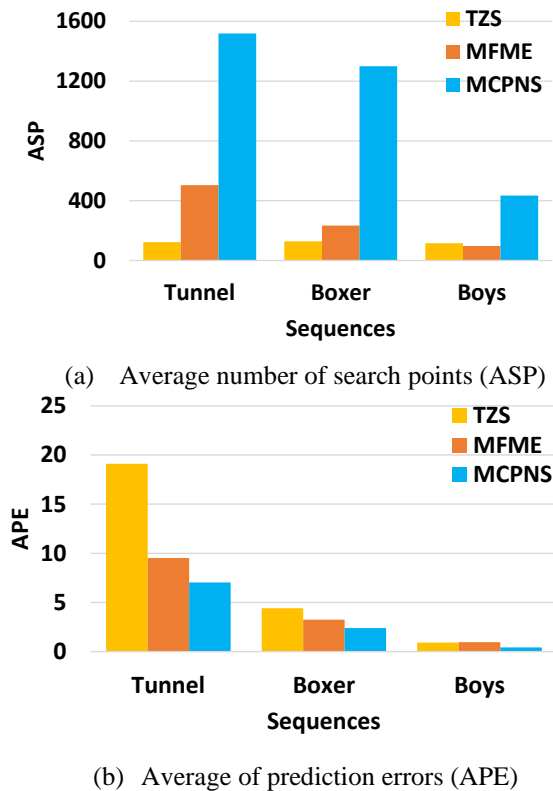


Fig. 13. A comparison of the average number of *ASP* and *APE* between various fast ME methods in several tested video sequences RA-main.

where N denotes the times of ME and $SP(i)$ represents the number of search points in i -th ME. We also evaluated the prediction accuracy of our proposed fast ME algorithm in terms of the *APE*, where the optimal MV was obtained by the FS method to measure the prediction error, as follows:

$$APE = \frac{\sum_{i=1}^N |MV_x^{Est}(i) - MV_x^{FS}(i)| + |MV_y^{Est}(i) - MV_y^{FS}(i)|}{N} \quad (11)$$

where N denotes the times of ME, and $MV^{Est}(i)$ and $MV^{FS}(i)$ denote the best MV estimated by the fast search method compared with the optimal MV obtained using the FS method in i th ME. The absolute difference error was calculated for the horizontal and vertical components of each MV. As illustrated in Fig. 13, we provide the *ASP* and *APE* measurements of the TZS, MFME, and our method in LD-main and RA-main, respectively. Results for the MTSS method are absent as we only had the executable file of this method. From these results, the number of search points in the proposed algorithms was higher than the TZS and MFME. However, our method had a smaller prediction error in terms of *APE* values compared with other methods, which means that our method can identify superior optimal MVs, resulting in superior coding performance, as demonstrated in Tables IV and V.

2) *The effect of different configurations in our proposed method.* We present the results of the ablation study on the effect of key configurations in our proposed method in Tables VI, VII, and VIII. The following conclusions can be derived:

- *Without Neighbors MCP search.* In order to highlight the significance of our proposed neighbors MCP search, we

TABLE VI

ABLATION STUDY ON EFFECT OF DIFFERENT SEARCH LOCATIONS OF OUR METHOD IN RA-MAIN CONDITION

Methods	Combination of different search locations			
	(I)	(I)+(II)	(I)+(III)	(I)+(II)+(III)
Avg. BD-rate	-2.04%	-2.44%	-2.19%	-2.54%
Avg. Enc. Time	100	1.02	0.99	103%

(I) = MCP location; (II) = Neighbors MCP location; (III) = Refinement location.

TABLE VII

ABLATION STUDY ON EFFECT OF DIFFERENT SEARCH CONFIGURATIONS OF OUR METHOD IN RA-MAIN CONDITION

Method	MLA orientation-agnostic search pattern		
	Original MCP pattern	Hexagon pattern	Rhombus pattern
Avg. BD-rate	-2.67%	-2.28%	-2.54%
Avg. Enc. Time	106%	103%	103%

conducted a test by disabling different search locations in our method. The results of this test are presented in Table VI. In cases where we only searched MCP locations (referred to as search location I) or combined MCP locations with refinement locations (i.e., search locations I + III), the performance exhibited a significant drop in comparison to the original proposed method. This resulted in BD-rate losses of 0.50% and 0.35%, respectively, when compared to our original approach. The reason for this performance decrease was the failure to accurately estimate the optimal motion vectors, particularly in scenarios with substantial motion deviations around each MCP location.

• *Without Fast MCP Search:* To validate the contribution of fast MCP search, the performance between the original MCP search and fast MCP search patterns are presented in Table VIII. The coding performance of our proposed fast MCP search (cases 2 and 4) saw only small decreases compared with the testing cases using the original MCP search pattern (cases 1 and 3). However, when we enabled our proposed fast MCP pattern as in cases 2 and 4, we achieved considerable time savings compared with cases 1 and 3 (e.g., the time complexity was reduced by approximately 75%, as shown in Fig. 14). This demonstrates that fast MCP search plays an important role in our proposed method. When we compared the two possible fast MCP search patterns (e.g., hexagon vs. rhombus), the rhombus-based fast MCP search was superior. We therefore adopted the rhombus for our final method.

• *Without Fast Neighbors MCP Search:* A new test was conducted to assess performance in the absence of our proposed fast neighbors MCP search, with the results presented in Table VIII and Figure 14. It was evident that scenarios without our fast neighbors MCP search demanded a significant increase in computational resources. This was primarily due to the need to execute

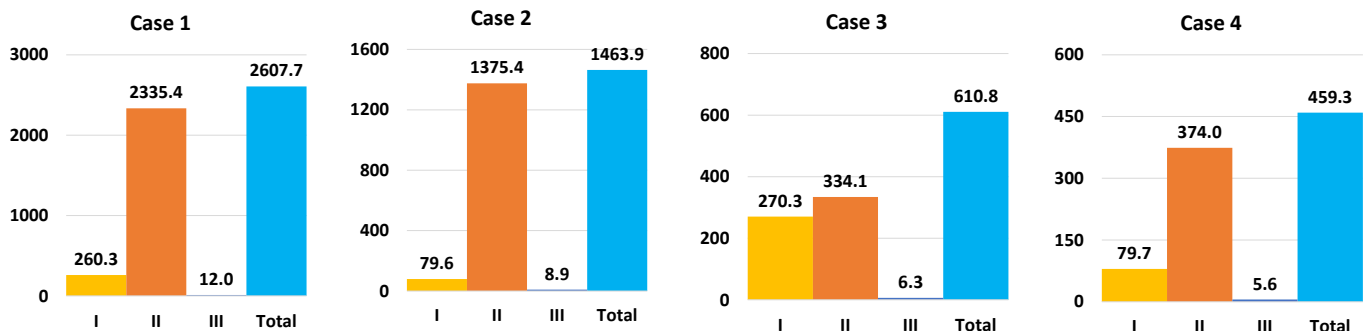


Fig. 14. Real-time consumption and its portion in each searching step in the Tunnel sequence at QP35 at RA-main condition. (I) MCP search location, (II) Neighbors MCP search location; (III) Refinement search location. (X-axis: search location, Y-axis: time in seconds).

TABLE VIII

ABLATION STUDY ON EFFECT OF DIFFERENT FAST SEARCH CONFIGURATIONS OF OUR METHOD IN RA-MAIN CONDITION

Search level Case number	MCP search locations		Neighbors MCP search locations		Average BD-rate (%)	Average Encoding Time (%)
	Original search candidates	Fast search candidates	Original search candidates	Fast search candidates		
Case 1	O	X	O	X	-2.69%	115%
Case 2	X	O	O	X	-2.49%	107%
Case 3	O	X	X	O	-2.67%	106%
Case 4	X	O	X	O	-2.54%	103%

*The highlighted row is the final method that we adopted as a in our paper

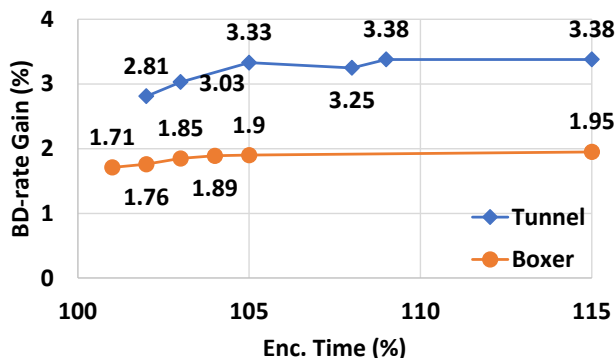


Fig. 15. Ablation tests on the parameter K number of neighbors MCP candidates, where there are six values of $K \in \{1, 2, 4, 8, 16, 32\}$ from the left to right of the diagram. In this paper, we adopted the $K = 16$ as the final setup.

the neighbors MCP search at every MCP location, resulting in a notable escalation in encoding time. For instance, when comparing the time consumption between case 1 and case 3 (or case 2 and case 4), encoding time increased by a factor of approximately 3 to 5 by checking all neighbors MCP location. Remarkably, the coding performance remained comparable to the original neighbors MCP search approach, highlighting the indispensable nature of our proposed fast neighbors MCP search in our method. Furthermore, Fig. 15 illustrates the ablation tests, demonstrating the effect of varying the K number of neighbors MCP search locations. It was observed that performance steadily improved as K increased. However, to strike a balance between performance and complexity, we adopted $K = 16$ in this paper.

3) *Extend the Motion Estimation Process in Both-Predictive Searches.* Bi-predictive motion estimation (BME) was carried out based on the results of uni-predictive motion estimation (UME), where the motion vector prediction (MVP) of the BME was set following the best estimated MV of each direction. The BME was used to obtain the optimal MV for each reference picture list: one is denoted as L0 (reference picture list 0) and the other as L1 (reference picture list 1). The BME combined two blocks to predict the current block by using an averaged weight approach.

Having established a fundamental understanding of the ME process, we implemented our proposed method in both uni-predictive and bi-predictive searches. The results, as presented in Table IX, showcased noticeable improvements in coding gains when compared to the TZS (VTM-11.0) anchor. Specifically, our method achieved BD-rate gains of approximately 2.54% and 2.90% in the context of uni-predictive and both-predictive searches, respectively. Additionally, in the RA-main condition, our method outperformed MTSS [58] by 0.82% in coding gains. These findings underscore the substantial coding advantages offered by our method, even in the absence of prior knowledge concerning MLA orientation. In pursuit of further optimizing the time complexity of our approach, we set the number of neighboring MCPs to $K = 4$. This configuration yielded bitrate savings of roughly 2.45% and 2.85% when our method was applied to uni-predictive and both-predictive searches, respectively, compared to the TZS method. Importantly, this optimization can reduce the time complexity of our method, as it remained comparable to that of the TZS method when $K = 4$.

TABLE IX

THE PERFORMANCE COMPARISON OF FAST ME METHODS USING IN BOTH-PREDICTIVE ME SEARCHES IN RA-MAIN CONDITIONS.

Camera model	Sequences	Applying in Uni-Predictive Search			Applying in Both-Predictive Search		
		MTSS* [58]	MCPNS (set K =16)	MCPNS (set K =4)	MTSS* [58]	MCPNS (set K =16)	MCPNS (set K =4)
Raytrix R5	Tunnel	-3.38%	-3.38%	-3.33%	-3.11%	-4.03%	-4.02%
	Fujita	-3.97%	-3.97%	-3.91%	-1.55%	-3.83%	-3.88%
	Origami	-4.51%	-4.51%	-4.43%	-2.68%	-4.65%	-4.58%
	Leading	-3.75%	-3.75%	-3.56%	-3.41%	-4.42%	-4.42%
Raytrix R8	Boxer	-1.90%	-1.90%	-1.89%	-1.84%	-2.80%	-2.70%
	ChessPieces	-4.64%	-4.64%	-4.29%	-4.44%	-5.21%	-5.14%
	ChessMoving	-4.75%	-4.75%	-4.79%	-5.46%	-5.87%	-5.81%
Single Focused	Boys	-0.25%	-0.25%	-0.26%	0.02%	-0.36%	-0.27%
	Experiments	-0.64%	-0.64%	-0.59%	-0.12%	-0.61%	-0.69%
	Cars	-0.03%	-0.03%	-0.04%	0.00%	-0.02%	-0.01%
	Matryoshka	-0.08%	-0.08%	0.16%	-0.30%	-0.08%	0.15%
Avg. BD-rate		-1.78%	-2.54%	-2.45%	-2.08%	-2.90%	-2.85%
Avg. Enc. Time Ratio		107%	103%	100%	109%	105%	101%

*The results generated using an executable file provided by the authors

V. CONCLUSIONS AND FUTURE WORKS

In this paper, we introduced a novel and efficient motion search algorithm designed for plenoptic 2.0 video coding. Beginning with a theoretical examination and motion statistical analysis of 4D LF images, we initially highlighted the fundamental distinctions in motion characteristics between traditional and plenoptic videos, along with distinctions in the motion behavior generated by plenoptic 1.0 and 2.0 cameras. Subsequently, we proposed fast and effective search patterns tailored to manage the complex motion behavior observed in the encoding of plenoptic 2.0 videos. Our experiments verified the effectiveness of the proposed algorithm in terms of coding performance and computational complexity. While our method showcased superior coding performance when compared to state-of-the-art methods, it is worth to mention that the time complexity of our approach remains relatively high. In the future, we plan to explore the development of a simplified search pattern or an early skip motion estimation method that can help reduce encoding time, especially in specific application scenarios.

REFERENCES

- [1] G. Wu, et al., "Light field image processing: An overview," *IEEE J. Sel. Topics Signal Process.*, vol. 11, no. 7, pp. 926–954, Oct. 2017.
- [2] C. Conti, L. D. Soares, and P. Nunes, "HEVC-based 3D holoscopic video coding using self-similarity compensated prediction," *Signal Process., Image Commun.*, vol. 42, pp. 59–78, Mar. 2016.
- [3] Y. Li, M. Sjostrom, R. Olsson, and U. Jennehag, "Coding of focused plenoptic contents by displacement intra prediction," *IEEE Trans. Circuits Syst. Video Technol.*, vol. 26, no. 7, pp. 1308–1319, Jul. 2016.
- [4] R. J. S. Monteiro, P. J. L. Nunes, N. M. M. Rodrigues, and S. M. M. Faria, "Light field image coding using high-order intra block prediction," *IEEE J. Sel. Topics Signal Process.*, vol. 11, no. 7, pp. 1120–1131, Oct. 2017.
- [5] C. Conti, P. Nunes, and L. D. Soares, "Light field image coding with jointly estimated self-similarity bi-prediction," *Signal Process. Image Commun.*, vol. 60, pp. 144–159, Feb. 2018.
- [6] X. Jin, H. Han, and Q. Dai, "Image Reshaping for Efficient Compression of Plenoptic Content," *IEEE J. Sel. Top. Signal Process.*, vol. 11, no. 7, pp. 1173–1186, 2017.
- [7] X. Jin, H. Han, and Q. Dai, "Plenoptic image coding using macropixel-based intra prediction," *IEEE Trans. Image Process.*, vol. 27, no. 8, pp. 3954–3968, 2018.
- [8] L. Li, X. Jin, and T. Zhong, "Imaging-correlated intra prediction for plenoptic 2.0 video coding," in *2020 IEEE International Conference on Multimedia and Expo (ICME)*, 2020.
- [9] X. Jin, et al., "Plenoptic 2.0 intra coding using imaging principle," *IEEE Trans. On Broadcast.*, vol. 68, no. 1, pp. 110–122, 2022.
- [10] E. Dib, et al., "Local low rank approximation with a parametric disparity model for light field compression," *IEEE Trans. Image Process.*, vol. 29, pp. 9641–9653, 2020.
- [11] M. Rizkallah, X. Su, T. Maugey, and C. Guillemot, "Geometry-aware graph transforms for light field compact representation," *IEEE Trans. Image Process.*, vol. 29, pp. 602–616, 2020.
- [12] G. De Oliveira Alves, et al., "The JPEG Pleno light field coding standard 4D-transform mode: How to design an efficient 4D-native codec," *IEEE Access*, vol. 8, pp. 170807–170829, 2020.
- [13] D. Liu, et al., "Pseudo-sequence-based light field image compression," in *Proc. IEEE Inter. Conf. on Multi. & Expo Workshops (ICMEW)*, 2016.
- [14] T. Nguyen Canh, V. V. Duong, and B. Jeon, "Boundary handling for video-based light field coding with a new hybrid scan order," in *Inter. Workshop on Adv. Image Tech. (IWAIT)*, 2019.
- [15] G. Wang, W. Xiang, M. Pickering, and C. W. Chen, "Light field multi-view video coding with two-directional parallel inter-view prediction," *IEEE Trans. Image Process.*, vol. 25, no. 11, pp. 5104–5117, Nov. 2016.
- [16] V. Avramelos, J. D. Praeter, G. V. Wallendael, and Lambert, P., "Random access prediction structures for light field video coding with MV-HEVC," *Multi. Tools and Applications*, vol. 79, pp. 12847–12867, May. 2020.
- [17] W. Tu, et al., "Efficient Content Adaptive Plenoptic Video Coding," *IEEE Access*, vol. 8, pp. 5797–5804, Jan. 2020.
- [18] T. H. Nguyen, V. V. Duong, B. Jeon, "Random-access-aware Light Field Video Coding using Tree Pruning Method," in *Proc. IEEE Inter. Conf. Visual Communi. and Image Processing*, 2020, pp. 128–131.
- [19] N. Mehajabin, et al., "An efficient pseudo-sequence-based light field video coding utilizing view similarities for prediction structure," *IEEE Trans. Circuits Syst. Video Technol.*, vol. 32, no. 4, pp. 2356–2370, 2022.
- [20] T. N. Huu, V. V. Duong, J. Yim, and B. Jeon, "Ray-space motion compensation for lenslet plenoptic video coding," *IEEE Trans. Image Process.*, vol. 32, pp. 1215–1230, 2023.
- [21] L. Li, Z. Li, B. Li, D. Liu, and H. Li, "Pseudo-sequence-based 2-D hierarchical coding structure for light-field image compression," *IEEE J. Sel. Top. Signal Process.*, vol. 11, no. 7, pp. 1107–1119, 2017.
- [22] J. Hou, J. Chen, and L.-P. Chau, "Light field image compression based on bi-level view compensation with rate-distortion optimization," *IEEE Trans. Circuits Syst. Video Technol.*, vol. 29, no. 2, pp. 517–530, 2019.
- [23] Jie Chen, Junhui Hou, and Lap-Pui Chau, "Light field compression with disparity-guided Sparse Coding based on Structural Key Views," *IEEE Trans. Image Process.*, vol. 27, no. 1, pp. 314–324, 2018.
- [24] X. Huang, P. An, Y. Chen, D. Liu, and L. Shen, "Low bitrate light field compression with geometry and content consistency," *IEEE Trans. Multimedia*, vol. 24, pp. 152–165, 2022.
- [25] D. Liu, P. An, R. Ma, W. Zhan, X. Huang, and A. A. Yahya, "Content-based light field image compression method with Gaussian process regression," *IEEE Trans. Multimedia*, vol. 22, no. 4, pp. 846–859, 2020.

- [26] F. Jiang, X. Jin, and T. Zhong, "Zoomable Intra Prediction for Multi-Focus Plenoptic 2.0 Video Coding," in *Proc. IEEE International Conference on Image Processing (ICIP)*, 2021.
- [27] F. Jiang, X. Jin, and K. Tong, "Pixel gradient based zooming method for plenoptic intra prediction," in *Proc. International Conference on Visual Communications and Image Processing (VCIP)*, 2021.
- [28] K. Tong, X. Jin, Y. Yang, C. Wang, J. Kang, and F. Jiang, "Learned Focused Plenoptic Image Compression with Microimage Preprocessing and Global Attention," in *IEEE Trans. Multimedia*, (Early Access), 10.1109/TMM.2023.3272747
- [29] C. Conti, L. D. Soares, and P. Nunes, "Dense Light Field Coding: A Survey," *IEEE Access*, vol. 8, pp. 49244-49284, March. 2020.
- [30] C. Brites, J. Ascenso, and F. Pereira, "Lenslet Light Field Image Coding: Classifying, Reviewing and Evaluating," *IEEE Trans. Circuits Syst. Video Technol.*, vol. 31, no. 1, pp. 339-354, Jan. 2021.
- [31] N00011, "Activity Report on Dense Light Fields", *132th MPEG meeting of ISO/IEC JTC1/SC29/WG11*, Online, October, 2020.
- [32] X. Jin, L. Li, T. Zhong, "Exploration of Lenslet Data Compression", *ISO/IEC JTC1/SC29/WG11 MPEG2018/M44685*, Macao, China.
- [33] F. Jiang, X. Jin, and T. Zhong, "Exploration Experiment of Plenoptic 2.0 test sequences for Dense Light Field Compression and Summary of Performance", *ISO/IEC JTC1/SC29/WG11 MPEG2020/M52249*, Brussels, Belgium January 2020.
- [34] X. Jin, K. Tong, E. S. Jang, T. Fujii, G. Lafruit, and M. Teratani, "Draft Use Cases and Requirements of Lenslet Video Coding (LVC) for Dense Light Fields (DLF)", *ISO/IEC JTC 1/SC 29/WG 2 N167*, January 2022.
- [35] S. Fujita, S. Mikawa, M. Teratani, K. Takahashi, and T. Fujii "Extracting Multi-View Images from Multi-Focused Plenoptic Camera". in *Proc. Inter. Workshop on Advanced Image Technology (IWAIT) 2019*.
- [36] M. Teratani, S. Fujita, W. Ouyang, K. Takahashi, and T. Fujii "3D Imaging System Using Multi-Focus Plenoptic Camera and Tensor Display", *International Conference on 3D Immersion (IC3D2018)*.
- [37] S. Fachada, D. Bonatto, A. Losfeld, G. Lafruit, and M. Teratani, "Pattern-free Plenoptic 2.0 Camera Calibration", in *Proc. IEEE 24th International Workshop on Multimedia Signal Processing MMSP*.
- [38] S. Fachada, A. Losfeld, T. Senoh, G. Lafruit, and M. Teratani, "A Calibration Method for Subaperture Views of Plenoptic 2.0 Camera Arrays", in *Proc. Inter. Workshop on Multi. Signal Process. MMSP 2021*.
- [39] X. Jin, L. Li, T. Zhong, "Exploration of Lenslet Data Compression", *ISO/IEC JTC1/SC29/WG11 MPEG2018/M44685*, Macao, China.
- [40] X. Jin, C. Wang, and K. Tong, "Summary of evidence in lenslet coding", *ISO/IEC JTC1/SC29/WG11 MPEG2021/M56790*, Online.
- [41] Y. Yu, X. Jin, C. Wang, K. Tong, and C. Wang, "[LVC][DLF] Integrated coding tools for the lenslet video on HEVC", *ISO/IEC JTC1/SC29/WG11 MPEG2022/M60183*, Online.
- [42] C. Wang, et al., "Integrated coding tools for the lenslet video on VVC", *ISO/IEC JTC1/SC29/WG4 MPEG2022/m60996*, Online.
- [43] K. Tong, X. Jin, F. Jiang, T. Zhong, and C. Wang, "[DLF] Transfer the inter coding tool for lenslet video compression to VVC", *ISO/IEC JTC1/SC29/WG4 MPEG2021/M56785*, Online.
- [44] J. Jain and A. Jain, "Displacement measurement and its application in interframe image coding," *IRE Trans. Commun. Syst.*, vol. 29, no. 12, pp. 1799-1808, 1981.
- [45] T. Koga, et al., "Motion-compensated interframe coding for video conference," *ITE Technical Report*, vol. 5, no. 9, pp. 85-90, 1981.
- [46] R. Li, B. Zeng, and M. L. Liou, "A new three-step search algorithm for block motion estimation," *IEEE Trans. Circuits Syst. Video Technol.*, vol. 4, no. 4, pp. 438-442, 1994.
- [47] L.-M. Po and W.-C. Ma, "A novel four-step search algorithm for fast block motion estimation," *IEEE Trans. Circuits Syst. Video Technol.*, vol. 6, no. 3, pp. 313-317, 1996.
- [48] L.-K. Liu and E. Feig, "A block-based gradient descent search algorithm for block motion estimation in video coding," *IEEE Trans. Circuits Syst. Video Technol.*, vol. 6, no. 4, pp. 419-422, 1996.
- [49] S. Zhu and K. K. Ma, "A new diamond search algorithm for fast block-matching motion estimation," *IEEE Trans. Image Process.*, vol. 9, no. 2, pp. 287-290, 2000.
- [50] C. Zhu, et al., "A novel hexagon-based search algorithm for fast block motion estimation," in *Proc. IEEE Inter. Conf. on Acoustics, Speech, and Signal*, 2002.
- [51] M. Tourapis, O.C. Au, M.L. Liou, "Fast Block Matching Motion Estimation using Predictive Motion Vector Field Adaptive Search Technique". *ISO/IEC/JTC1/SC29/WG11 MPEG2000/M5866,2000*
- [52] Z. Chen, P. Zhou, Y. He. "Fast Integer Pel and Fractional Pel Motion Estimation for JVT", *Joint Video Team (JVT) of ISO/IEC MPEG & ITU-T VCEG*, December, 2002.
- [53] G. J. Sullivan, et al., "Overview of the high efficiency video coding (HEVC) standard," *IEEE Trans. Circuits Syst. Video Technol.*, vol. 22, no. 12, pp. 1649-1668, 2012.
- [54] L. Li, X. Jin, H. Han, and Q. Dai, "Macropixel based Fast Motion Estimation for Plenoptic Video Compression" in *Proc. Pacific-rim Conf. Multimedia*, vol. 3, pp. 730-739, 2018.
- [55] L. Li, and X. Jin, "Macropixel-constrained Collocated Position Search for Plenoptic Video Coding," *Proc. IEEE Inter. Conf. Visual Comm. and Image Processing*, 2020, pp. 1-4.
- [56] T. N. Huu, V. V. Duong, and B. Jeon, "Fast and efficient microlens-based motion search for plenoptic video coding," in *Proc. IEEE Inter. Conference on Image Processing (ICIP)*, 2021.
- [57] Y. Yim, T. N. Huu, and B. Jeon, "[LVC][DLF] Fast and efficient microlens-based motion search for Lenslet Video Coding", *ISO/IEC JTC1/SC29/WG11 MPEG2022/M60992*, Online.
- [58] Y. Yang, X. Jin, K. Tong, C. Wang and H. Huang, "Microimage-based Two-step Search For Plenoptic 2.0 Video Coding," in *Proc. IEEE Inter. Conf. on Multimedia and Expo (ICME)*, 2023, pp. 2567-2572.
- [59] Y. Yu, X. Jin, C. Wang, and K. Tong, "[LVC][DLF] Improved Test Zone Search for Plenoptic 2.0 video coding", *ISO/IEC JTC1/SC29/WG11 MPEG2022/M60995*, Online.
- [60] Y. Yang, X. Jin, C. Wang, K. Tong, and H. Huang, "Micro-image Correlative Block Search for Plenoptic 2.0 video coding", *ISO/IEC JTC1/SC29/WG4 MPEG2022/M60997*, Online.
- [61] Y. Yang, X. Jin, C. Wang, K. Tong, and H. Huang, "Microimage-based Two-step Search for Plenoptic 2.0 Video Codings", *ISO/IEC JTC1/SC29/WG4 MPEG2022/M61861*, Online.
- [62] Y. Yang, X. Jin, K. Tong, C. Wang, and H. Huang, "[DLF] [LVC] Updated Performance of Microimage-based Two-step Search for Plenoptic 2.0 Video Coding," *ISO/IEC JTC 1/SC 29/WG 4 m62934*, Antalya, April 2023.
- [63] Y. Yang, X. Jin, K. Tong, and C. Wang, "[LVC] [DLF] Low-complexity Microimage-based Two-step Search for Plenoptic 2.0 Video Coding", *ISO/IEC JTC 1/SC 29/WG 4 MPEG2023/M64053*, Geneva, July 2023.
- [64] J. Luo, J. Ye, Q. Liu, and Y. Yang, "[LVC][DLF] Macro-pixel level and pixel level mixed search for plenoptic 2.0 videos", *ISO/IEC JTC 1/SC 29/WG 4 MPEG2023/M63160*, Antalya, Turkey, April 2023.
- [65] J. Luo, J. Ye, Q. Liu, and Y. Yang, "[LVC][DLF] Macropixel-constrained Collocated Position Layered Search for Plenoptic 2.0 Videos", *ISO/IEC JTC 1/SC 29/WG 4 MPEG2023/M64075*, Geneva, July 2023.
- [66] J. Yim, V. V. Duong, T. N. Huu, and B. Jeon, "[LVC][DLF] Fast and Efficient Macropixel Collocated Pixel Search for Plenoptic 2.0 Video Coding", *ISO/IEC JTC 1/SC 29/WG 4 MPEG2023/M63315*, Antalya, April 2023.
- [67] J. Yim, V. V. Duong, T. N. Huu, and B. Jeon, "[LVC][DLF] Improving Macropixel Collocated Position Search for Plenoptic 2.0 Video Coding", *ISO/IEC JTC 1/SC 29/WG 4 MPEG2023/M63908*, Geneva, July 2023.
- [68] J. Yim, V. V. Duong, T. N. Huu, and B. Jeon, "[LVC][DLF] Further Improving Macropixel Collocated Position Search for Plenoptic 2.0 Video Coding", *ISO/IEC JTC 1/SC 29/WG 4 MPEG2023/M64788*, Hanover, October 2023.
- [69] S. Ma, B. M. Smith, and M. Gupta, "3D scene flow from 4D light field gradients," in *Proc. ECCV 2018*, pp. 681-698.
- [70] A. Lumsdaine and T. Georgiev, "The focused plenoptic camera," in *Proc. IEEE Inter. Conf. on Computational Photography (ICCP)*, 2009, pp. 1-8.
- [71] M. Levoy and P. Hanrahan, "Light field rendering," in *Proc. Annual Conf. Comp. Graph. and Inter.e Techni.*, in *Proc. SIGGRAPH*, 1996, pp. 31-42.
- [72] S. Gortler, R. Grzeszczuk, R. Szeliski, and M. Cohen, "The lumigraph," in *Proc. SIGGRAPH*, 1996, pp. 43-54.
- [73] F. Bossen, Common Test Conditions and Software Reference Configurations, *JCT-VC, doc. JCTVC-11100*, May 2012.
- [74] VVC reference software VTM-11.0 [Online]. Available at https://vcgit.hhi.fraunhofer.de/jvet/VVCSoftware_VTM/-/tags/VTM-11.0
- [75] Exploration Experiments and Common Test Conditions for Dense Light Fields, *ISO/IEC JTC 1/SC 29/WG 04, MDS20009_WG04_N00057*, Online, January 2021.
- [76] G. Bjontegaard, "Calculation of average PSNR differences between RDcurves," *ITU-T SG16 Q.6, VCEG-M33, VCEG of ITU-T, Austin, Texas, USA, Tech. Rep. VCEG-M33*, Apr. 200.